PNAS Nexus, 2024, 3, 1–6
https://doi.org/10.1093/pnasnexus/pgae086
Advance access publication 19 February 2024
Research Report

Directed droplet motion along thin fibers

Hamza K. Khattak[a], Aileen Shanzeela[a], Elie Raphael[b] and Kari Dalnoki-Veress[a,b,*]

[a]Department of Physics and Astronomy, McMaster University, Hamilton, ON L8S 4L8, Canada
[b]UMR CNRS Gulliver 7083, ESPCI Paris, PSL Research University, Paris 75005, France
*To whom correspondence should be addressed: Email: dalnoki@mcmaster.ca
Edited By: Cristina H. Amon

Abstract

When microscopic droplets are placed between fibers held at a fixed angle, the droplets spontaneously move toward the apex of the fibers. The speed of the droplet motion increases both with the angle between the fibers and the distance the droplet spans across the fibers. The speed of these droplets can be described by a simple scaling relationship. Bending these fibers into a sawtooth geometry results in a droplet ratchet where cyclic motion in a fiber results in extended linear motion of the droplet, and can even be used to induce droplet mergers.

Keywords: droplets, fibers, microfluidics

Significance Statement

Transportation of microscopic droplets is important in many natural and engineered systems, from cacti using their needles for water harvesting to microfluidic devices used to encapsulate and deliver medicines. We have developed a system where we can control the motion of droplets using thin fibers held at fixed angles. Droplets migrate spontaneously to the meeting point of two fibers, and the motion can be explained with a simple model. Based on these principles, a rigid fiber is bent into a specific pattern which allows rapid motion of droplets over large distances using a ratchet-like motion. The mechanism by which droplet motion is achieved is versatile and can accomplish complex and selective motion of droplets relevant in microfluidic applications.

Introduction

When a cactus needle is placed in a foggy environment, the needle will collect droplets which spontaneously migrate toward the plant stems (1, 2). Conversely, fibers in the fur of otters prevent water transportation and allow the otter to remain warm in arctic conditions (3). The wide range of interactions between liquids and fibers has naturally resulted in a host of applications seeking to replicate nature (4–7) and there has been great interest in understanding the physics of such systems. The ideal case of a single droplet wetting a single stiff fiber has been well studied (8, 9). Depending on the size of droplet, the size of the fiber, and the interfacial tensions involved, the liquid will adopt either an axisymmetric barrel-like or clam-shell configuration on the fiber (9). Yet even with a single fiber, adding additional parameters can immediately introduce significant complexity (10–17). For example, a flexible fiber may coil around or within a droplet (18–21) and a fiber with a gradient in the radius is what causes droplet motion in cactus needles (1, 22).

With such varied behavior in single fiber systems, the difficulty in understanding how droplets interact with multiple fibers becomes clear. Therefore, it has not been until more recently that there have been great advances in the study of droplets interacting with fiber arrays, often driven by fundamental interests, but also to improve applications like fog harvesting. Work has ranged from studying how droplets interact with fiber pairs (23–32) to large grids of fibers (33–36). For example, capillary forces can bring two fibers together causing droplets to move toward the open end (25), similar to the case of a droplet between plates (37). Recent work has also shown that bent fibers can effect how much liquid is supported before droplets fall due to gravity (30). In grids, varying the fiber thickness in different strands of the grid can be used to pattern droplets (35).

Here, we report on droplets placed between thin stiff fibers held at some angle as shown in Fig. 1. We find that a droplet migrates toward the apex of the fibers and develop a simple scaling model that describes the droplet motion. In general, geometric limitations in droplet–fiber systems mean the distance the droplet can be transported is limited by the diameter of the droplet. We overcome this limitation with a droplet ratchet mechanism that can transport droplets across long distances, independent of droplet size, by coupling a straight fiber and a fiber with alternating bends. Lastly, we illustrate that the ratchet mechanism, and a conceptually similar alternative, can both be used to initiate droplet mergers.

Competing Interest: The authors declare no competing interest.
Received: January 25, 2024. **Accepted:** February 1, 2024

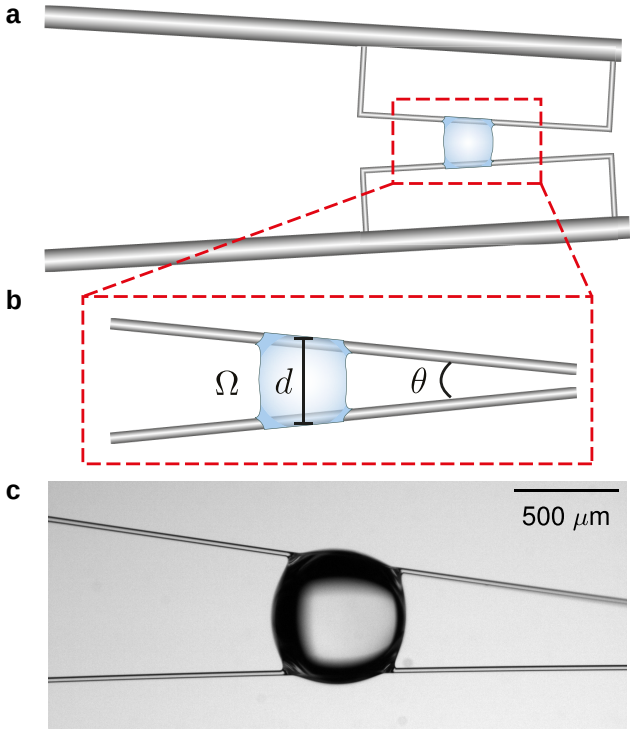

Fig. 1. a) Sketch of the experimental setup. A silicone oil droplet is placed between two thin glass C-shaped fibers, which are mounted onto thicker glass rods. The C-shaped fibers are glued at both ends to the thicker rods to ensure minimal deflection due to capillary forces. b) Expanded view of the experiment with the relevant parameters indicated, Ω is the volume, d is the distance spanned by the fibers, and θ is the angle between the fibers. c) A typical image of the droplet between the two fibers. These images are viewed from above, with the fibers in the horizontal plane.

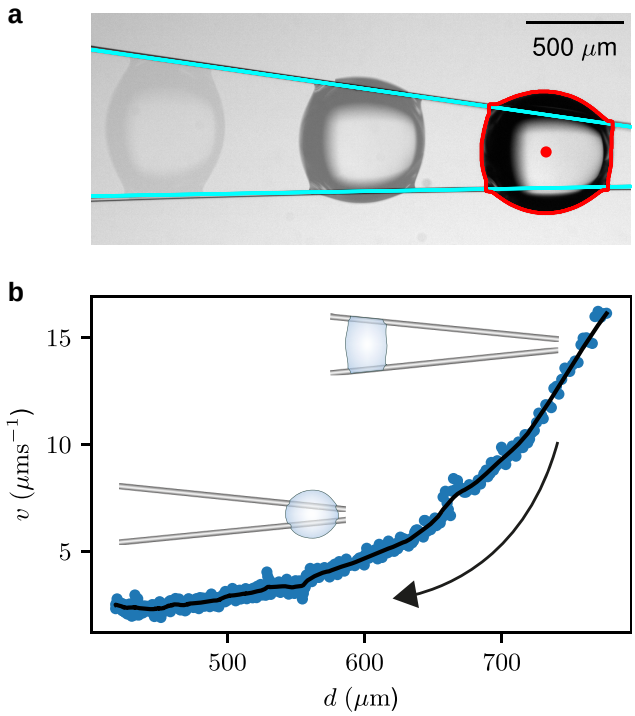

Fig. 2. a) Image showing three snapshots of the droplet through time (t = 0, 35, 98 s). The droplet moves from left to right toward the apex. The blue lines (lines going through the fibers) show position tracking for the fibers, the red line (line along the perimeter of the droplet) shows the edge of the droplet, and the central red dot the position of the droplet. The position is defined by the averaged location of all pixels within the red line. b) Plot of droplet speed as a function of the distance between between the fibers at the position of the droplet center. We note that the droplet moves toward the apex, thus from the right (large d) to left (small d) in this plot (sketches of typical configurations are inset).

Experimental setup

To study the interaction between the droplet and rigid fibers, we design an idealized system such that we can assume that only capillary interactions and viscous dissipation are important. We use small droplets with radius $r_d \sim 100\,\mu$m. Since the droplets are smaller than the capillary length, we can ignore gravity. A further simplification can be made by ensuring that the fibers are small compared to the droplet. Since the droplets are small, the fibers need to be thin, with radius $r_f \sim 10\,\mu$m. For most materials, sufficiently long fibers with this radius held at one end would deform significantly due to capillary forces from the droplet, and hence alter the angle we try to control. To avoid this, we use the glass fiber system shown in Fig. 1a. Full details of the manufacturing are described in Fig. S1. Briefly, thin glass fibers are heated and pulled from rods to diameters $\sim 10\,\mu$m. A home-built microforge is used to bend the fibers into rectangular C shapes. These fibers are then bonded to much thicker rods (1mm diameter) to maximize stiffness. With the rectangular C-shaped fibers, the fiber bending from capillary forces remains minimal at $\sim 0.1^\circ$ or $\sim 1\,\mu$m deflection for a $\approx 1{,}000\,\mu$m fiber length (see Fig. S2).

For the droplets, we use silicone oil (1,000 cSt, Gelest), which is chosen for two reasons. First, the silicone oil is nonvolatile which allows for longer timescale experiments. Second, silicone completely wets the fibers reducing the possibility of pinning, thereby allowing measurements even when the driving force is low.

To control the fibers at small lengthscales, we use a custom goniometer that can precisely control the angle between the fibers while keeping a point of interest within a $\sim 10\,\mu$m^2 area (see Fig. S3). With the two fibers positioned, a droplet is deposited. The process of droplet deposition involves first dip coating a thin glass fiber (thinner than the fiber of interest) with the silicone oil. The coated fiber can then be slid across the fiber under study. Due to the reduced surface area, droplets bind more weakly to thinner fibers, which enables the transfer of a droplet from the coated fiber to the fiber of interest.

The droplet–fiber system is imaged from above and a sequence of images is used to track the droplet migration (see Movie S1). The droplet is found to migrate spontaneously toward the apex of the fibers (Fig. 2a). To quantify this motion, we use simple edge detection to track the center of the droplet cross-sectional area. With the droplet center location, we can determine the droplet speed as well as the distance the droplet bounds between the fibers (Fig. 2b and Movie S2).

To return the droplets to their original position, we simply rotate the fibers to a negative angle to reverse the direction of motion allowing us to repeat experiments. During droplet motion, the silicone oil leaves a thin Landau–Levich film on the fibers that increases with deposition speed (13, 38). To minimize the thickness and variability in the Landau–Levich film, the droplets are returned slowly ($v \lesssim 1\,\mu$m s^{-1}) at a shallow angle ($\theta \approx 1^\circ$), which results in a thin coating on the fiber with thickness $<1\,\mu$m. With this process, we are able to quantify how droplets move along fibers held at an angle.

Results and discussion

Scaling model and comparison to experiments

With the ability to measure the speed and span of the droplets, we can develop a simple scaling model for droplet motion. We have a

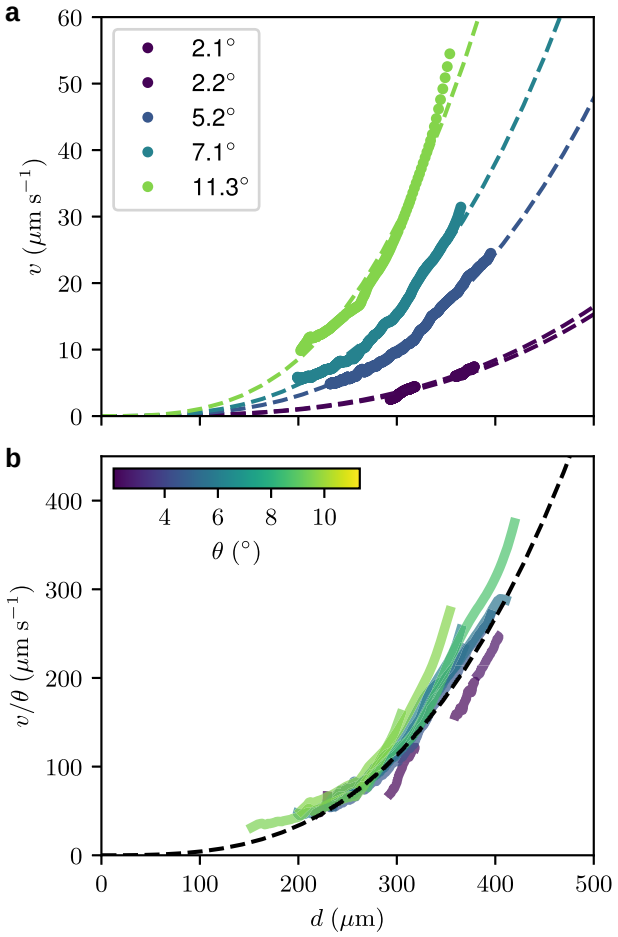

Fig. 3. a) Plot of the speed of a droplet ($\Omega = 18$ nL) as a function of its span for a selection of angles. The fits shown are to $v = ad^3$. b) Plot of speed normalized by angle in radians as a function of the distance spanned by the droplet. Note here that there are 11 different angles in this plot with the color-bar indicating the specific angle of each plot.

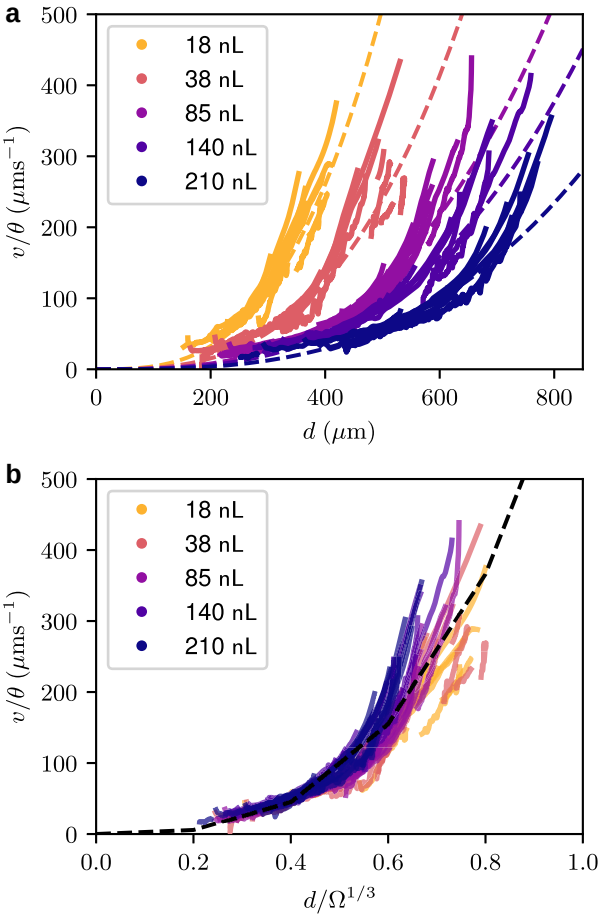

Fig. 4. a) Plot of speed normalized by angle as a function of the distance spanned by droplets for several different volumes. The data for each volume represent 10–15 separate angle experiments. Droplet volume is calculated by taking a volume of revolution of the droplet while symmetric on a single fiber. b) Plot of speed normalized by angle in radians as a function of the aspect ratio of the droplet for a series of volumes.

droplet with volume Ω, viscosity η, and surface tension γ, which contacts two thin fibers. The droplet fully wets the fiber. If we assume that the surface area of the droplet is much larger than the wetted interface of the droplet with the fiber (i.e. fiber diameter is $\ll \Omega^{1/3}$) then the free energy of the system is simply the product of the surface tension with the surface area of the droplet: $\gamma\mathcal{S}$. As shown in Fig. 1, the angle between the fibers is θ, the x coordinate is given by the symmetry-axis of the system, and the apex of the fibers defines $x = 0$. The distance between the fibers at the location of the droplet, $d(x)$, is $d(x) \approx x\theta$ for small θ which is valid for the experiments carried out. Because the surface-to-volume ratio decreases as the distance between the fibers decreases, the droplet migrates toward $x = 0$. The characteristic speed of the system is set by the capillary velocity γ/η.

The velocity of the droplet must depend on the parameters $\{d, \Omega, \theta, \eta, \gamma\}$, and we start with the simple ansatz that at the level of scaling we have

$$v \propto \frac{\gamma}{\eta}\left(\frac{d}{\Omega^{1/3}}\right)^{\alpha}\theta^{\beta}, \tag{1}$$

where the exponents α and β are to be determined. Since the surface area of the droplet for thin fibers and small angles only depends on Ω and d (assuming small angles), the capillary force driving the droplet to the apex depends on the gradient of the surface energy:

$$f_{\text{cap}} = \frac{\partial}{\partial x}[\gamma\mathcal{S}(\Omega, d)] \approx \gamma\theta\frac{\partial}{\partial d}[\mathcal{S}(\Omega, d)]. \tag{2}$$

With the kinematic viscosity, ν, the Reynolds number in the experiments is given by $\text{Re} \equiv vl/\nu \sim (10^{-4}\,\text{m s}^{-1})(10^{-3}\,\text{m})/(10^{-2}\,\text{m}^2\,\text{s}) \sim 10^{-5}$. Given that $\text{Re} \ll 1$, we can neglect inertial effects and the velocity is proportional to the driving force. Since $f_{\text{cap}} \propto v$, we obtain the exponent $\beta = 1$ and we have the experimentally testable scaling relationship

$$v \propto \frac{\gamma\theta}{\eta}\left(\frac{d}{\Omega^{1/3}}\right)^{\alpha}. \tag{3}$$

To test Eq. 3, we first perform experiments with a range of fiber angles, $\theta \in [2.1°, 11.3°]$, while keeping the volume fixed, $\Omega = 18$ nL. In Fig. 3a, the results of the droplet velocity as a function of the distance the droplet spans between the two fibers are shown. As the span decreases, so does the speed of the droplet (droplet is less deformed and closer to equilibrium the smaller the span). Furthermore, at a fixed span, the velocity increases with the angle, which is consistent with the expectation that the capillary driving force increases linearly with the angle (see Eq. 2).

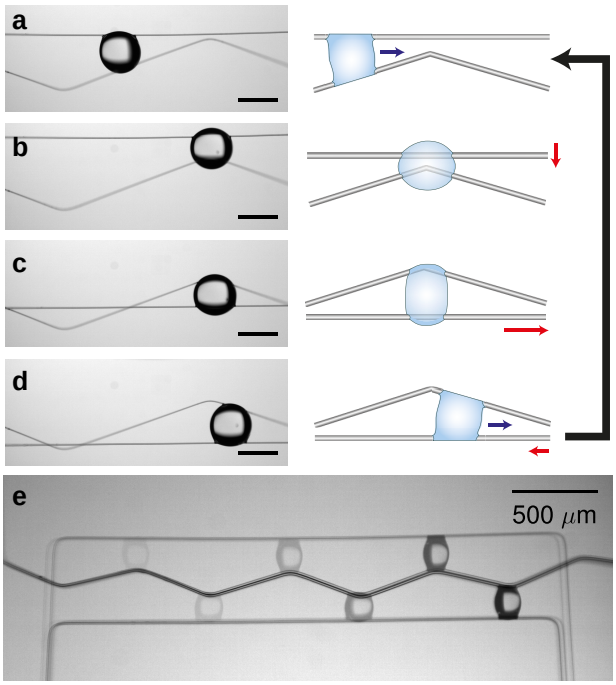

Fig. 5. Images and corresponding sketches of droplet migration driven by the ratchet mechanism (scalebars are 500 μm, see Movie S3). a) Droplet moving toward the apex. b) Droplet at the corner of a sawtooth, once at this point the straight fiber can be translated downwards to the other size of the sawtooth fiber. c) Droplet at point of unstable equilibrium, the straight fiber can be translated horizontally to initiate droplet motion in the desired direction. d) Droplet once again moving spontaneously toward the apex, at this step the straight fiber can be retracted horizontally to its original position. e) Overlaid images of droplet moving across several teeth of a sawtooth pattern, while both fibers return to their original position after each cycle (Movie S4).

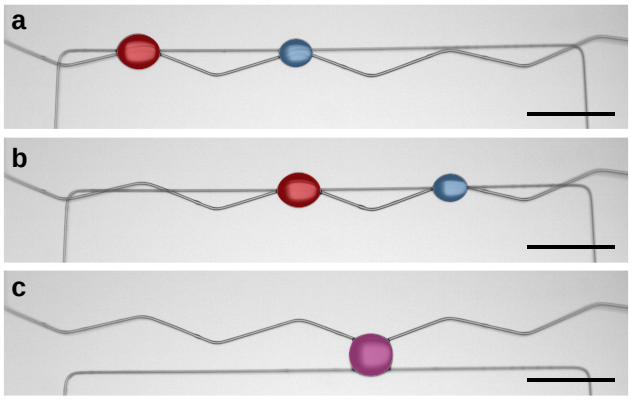

Fig. 6. Series of images showing the the use of a sawtooth pattern to first move droplets the same distance and then merge the droplets (Movie S5). The colors are guides to the eye to identify the left and right droplets. a) Initial location of droplets. b) Droplets are moved across one of the teeth in the sawtooth pattern, $t = 55$ s. c) The two droplets are merged, $t = 70$ s. All scalebars are 500 μm. Larger motions result in simultaneous motion where smaller motions allow for a merger. A detailed mechanism is outlined in Fig. S4.

The data in Fig. 3a are consistent with a power law in the span as expected from Eq. 3 with the exponent $\alpha \approx 3$, as shown by the best fit lines to the expression $v = ad^3$, with a a fit parameter. We note that a free fit to the data used for Fig. 3a gives $\alpha = 3.3 \pm 0.4$. For the largest angles, the match to power law starts to break down but the scaling still qualitatively matches the data. In Fig. 3b, we confirm the scaling dependence on the angle, θ, predicted by Eq. 3 by plotting v/θ as a function of the span, d, for 11 different experiments which is well described by a single curve ($v/\theta = bd^3$, with $b = 4.5 \pm 0.6\,\mathrm{mm^{-2}\ s^{-1}}$).

All the experiments discussed thus far (Fig. 3) are with a fixed volume. We next turn to the dependence of the dynamics on the droplet volume. Experiments were performed, just as shown in Fig. 3, but for a range of droplet volumes with $\Omega \in [18\,\mathrm{nL}, 210\,\mathrm{nL}]$. In Fig. 4a, we plot v/θ as a function of d for five volumes and at least 10 angles for each volume. We see that for a given speed, the smaller droplets move more quickly. This result is consistent with the intuition introduced above that a smaller droplet requires a larger aspect ratio (further from equilibrium) to span the same distance as a larger droplet. Lastly, guided by the scaling of Eq. 3, we plot the angle-normalized speed as a function of the aspect ratio $d/\Omega^{1/3}$, as shown in Fig. 4b (see Fig. S4 for data with varying fiber thickness). We find the data collapses reasonably well to a simple master curve given by the expression $v/\theta = c(d/\Omega^{1/3})^3$, with $c = 690 \pm 90\,\mu\mathrm{m\ s^{-1}}$. In Fig. S5, we generalize this procedure for other liquids and show that the scaling holds for both hydrophobic and hydrophilic liquids. Despite the assumptions made in the simple scaling model, the model well captures the essential physics of the motion of droplets between stiff fibers held at an angle.

Droplet ratchet

Now that we have an understanding of the physics at play, we can use the concepts to develop a droplet ratchet that turns cyclic motion of a fiber into linear motion of a droplet. The principle is simply to take advantage of the fact that the droplet will move to the apex. The ratchet system involves a placing droplet between a straight fiber and a sawtooth-shaped fiber (Fig. 5a). A sawtooth fiber is prepared through a series of bends in a thin glass fiber (Fig. S1). We align the bends in one plane and ensure a consistent angle between the bends. The sawtooth pattern consists of the straight portions that move toward or away from the other fiber and the corner portions where the fiber changes direction.

The mechanism of motion starts with a droplet between a straight fiber and a straight portion of sawtooth (Fig. 5a). Since the droplet is in between two fibers held at an angle it will move toward the apex, in this case the corner of a sawtooth (Fig. 5b). Once at the apex, we translate the straight fiber downwards to cross the sawtooth fiber (Fig. 5c). The first translation leaves the droplet in a place of unstable equilibrium. We then translate the straight fiber slightly in the intended direction of motion to break the symmetry, and the droplet begins moving in that direction (Fig. 5d). While this motion is happening, or when the droplet is in a stable equilibrium at step 2, the straight fiber can be retracted horizontally back to its original position. With once cycle complete the process can be repeated to further move the droplet (Movie S3).

Without any optimizations for speed, we are able to move highly viscous (1,000 cSt) nanoliter droplets at speeds of $\sim 100\,\mu\mathrm{m\ s^{-1}}$ over many droplet lengths (Fig. 5e and Movie S4). With this method, the magnitude of droplet motion is decoupled from the magnitude of each translation step required for motion. In principle, the sawtooth pattern could be repeated for whichever distance of droplet motion is desired, providing an effective method of transporting microdroplets across large distance without the pressure

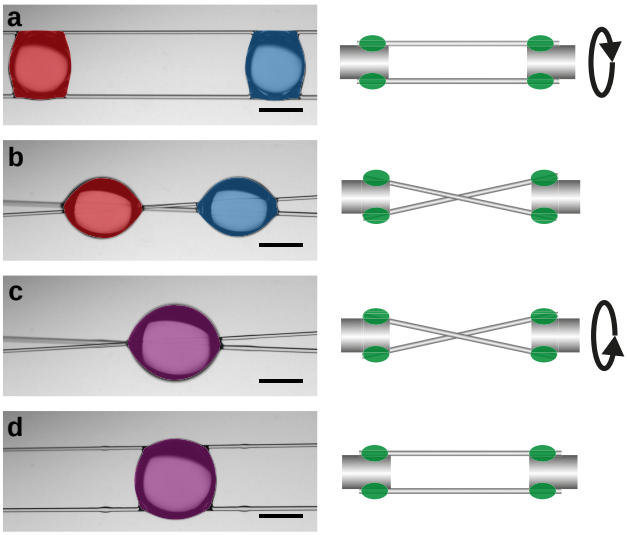

Fig. 7. Series of images and corresponding schematics showing the the use of a twisting mechanism to merge the droplets (Movie S6). All scalebars are 500 μm and the colors are guides to the eye to identify the left and right droplets. a) Initial location of droplets. b) Fibers are twisted from a parallel to crossed configuration. The droplets move toward the apex. c) The two droplets have merged after $t \sim 180$ s. d) The fibers return to the parallel configuration. See Fig. S6 for further details.

differentials required standard channel-based methods. Since there is flexibility in the fiber translation distances and speeds required for droplet motion (Fig. S8), the ratchet mechanism is easily automated.

In addition to moving a single droplet large distances, we can also use the same ratchet mechanism to selectively move or merge multiple droplets along a single sawtooth (Fig. 6). The detailed mechanism for the selective movement and merger process is outlined in Fig. S7. In brief, since the motion requirement to move a droplet out of unstable equilibrium depends on the size of the droplet, we can selectively move individual droplets by changing the extent of fiber motion. Using our selective ratchet mechanism technique it is possible to first move two droplets in the same direction, and then by changing motion parameters, have the droplets merge. We note that the ratchet mechanism is just one variation on a theme and is not the only method that exploits the flexibility of this fiber system for droplet transport. For example, we have exploited a variation of this theme whereby we rotate two fibers such that the system transitions from a parallel configuration to a crossed-fiber geometry (see Figs. 7 and S6). With this geometry, two droplets on the opposite side of the assembly can be reliably made to merge at the intersection of the fibers to generate droplet motion resulting in mergers.

Conclusion

With a combination of glass fiber manufacturing and microscale fiber control, we can study the motion of a droplet between two stiff fibers. We have developed a simple scaling model that describes the essential physics of the droplet–fiber system and explains why the droplet moves toward the apex of the two fibers. The geometry of fibers converging at an apex imposes a limit on the distance a droplet can traverse. To overcome this limitation, we propose a ratchet method that involves coupling a straight fiber with a sawtooth-shaped fiber, enabling the long-distance transportation of microdroplets.

We note that the combination of the sawtooth and straight fibers is just one example exploited here. Variations of this theme can be used to accomplish complex and selective motion of droplets, including, as we have shown, the mixing of droplets through mergers. Unlike traditional microfluidics, these mergers can be conducted with nanoliter quantities at atmospheric pressure, allowing for ultrasmall-scale chemistry. The ability to transport droplets over considerable distances has practical applications in diverse fields, ranging from large-scale fog harvesting to the development of a novel microfluidic platform.

Supplementary Material

Supplementary material is available at *PNAS Nexus* online.

Funding

H.K.K. and K.D.-V. acknowledge financial support from the Natural Science and Engineering Research Council of Canada and H.K.K. acknowledges funding from the Vanier Canada Graduate Scholarship.

Author Contributions

H.K.K. and K.D.-V. designed the experiments. A.S. ran initial experiments. H.K.K. ran experiments and completed analysis. E.R. and K.D.-V. developed the theory. H.K.K. wrote the first draft of the manuscript, with contributions from E.R. and K.D.-V.

Data Availability

The data underlying this work are available via the zenodo repository at https://doi.org/10.5281/zenodo.10652305.

References

1 Guo L, Tang GH. 2015. Experimental study on directional motion of a single droplet on cactus spines. *Int J Heat Mass Transf*. 84: 198–202.
2 Ju J, *et al*. 2012. A multi-structural and multi-functional integrated fog collection system in cactus. *Nat Commun*. 3(1):1247.
3 Liwanag HEM, Berta A, Costa DP, Abney M, Williams TM. 2012. Morphological and thermal properties of mammalian insulation: the evolution of fur for aquatic living. *Biol J Linn Soc*. 106(4): 926–939.
4 Li K, *et al*. 2013. Structured cone arrays for continuous and effective collection of micron-sized oil droplets from water. *Nat Commun*. 4(1):2276.
5 Bai F, Wu J, Gong G, Guo L. 2015. biomimetic "cactus spine" with hierarchical groove structure for efficient fog collection. *Adv Sci*. 2(7):1500047.
6 Wilson JL, *et al*. 2023. How drops of liquid move along parallel fibres in a perpendicular airflow. *Nat Phys*. 19:1565–1566.
7 Bintein P-B, Bense H, Clanet C, Quéré D. 2019. Self-propelling droplets on fibres subject to a crosswind. *Nat Phys*. 15(10):1027–1032.
8 de Gennes P-G, Brochard-Wyart F, Quéré D. 2004. *Capillarity and wetting phenomena*. New York (NY): Springer.
9 McHale G, Newton MI. 2002. Global geometry and the equilibrium shapes of liquid drops on fibers. *Colloids Surf. A Physicochem Eng Asp*. 206(1):79–86.
10 Abishek S, Mead-Hunter R, King AJC, Mullins BJ. 2019. Capture and re-entrainment of microdroplets on fibers. *Phys Rev E*. 100(4):042803.

11 Van de Velde P, Protière S, Duprat C. 2021. Dynamics of drop absorption by a swelling fiber. *Soft Matter*. 17(25):6168–6175.
12 Jamali M, Tafreshi HV. 2021. Studying droplet adhesion to fibers using the magnetic field: a review paper. *Exp Fluids 2021 628*. 62(8):1–15.
13 Lee CL, Chan TS, Carlson A, Dalnoki-Veress K. 2022. Multiple droplets on a conical fiber: formation, motion, and droplet mergers. *Soft Matter*. 18(7):1364–1370.
14 Gao X, Jiang L. 2004. Water-repellent legs of water striders. *Nature*. 432(7013):36.
15 Chan TS, Yang F, Carlson A. 2020. Directional spreading of a viscous droplet on a conical fibre. *J Fluid Mech*. 894:A26.
16 Chan TS, Lee CL, Pedersen C, Dalnoki-Veress K, Carlson A. 2021. Film coating by directional droplet spreading on fibers. *Phys Rev Fluids*. 6(1):014004.
17 Chan TS, Pedersen C, Koplik J, Carlson A. 2021. Film deposition and dynamics of a self-propelled wetting droplet on a conical fibre. *J Fluid Mech*. 907:A29.
18 Roman B, Bico J. 2010. Elasto-capillarity: deforming an elastic structure with a liquid droplet. *J Condens Matter Phys*. 22(49):493101.
19 Elettro H, Neukirch S, Vollrath F, Antkowiak A. 2016. In-drop capillary spooling of spider capture thread inspires hybrid fibers with mixed solid–liquid mechanical properties. *Proc Natl Acad Sci U S A*. 113(22):6143–6147.
20 Schulman RD, *et al*. 2017. Elastocapillary bending of microfibers around liquid droplets. *Soft Matter*. 13(4):720–724.
21 Fortais A, Charlesworth K, Schulman RD, Dalnoki-Veress K. 2021. Spontaneous elastocapillary winding of thin elastic fibers in contact with bubbles. *Phys Rev Lett*. 127(21):218001.
22 Lorenceau É, Quéré D. 2004. Drops on a conical wire. *J Fluid Mech*. 510:29–45.
23 Wu X-F, Bedarkar A, Vaynberg KA. 2010. Droplets wetting on filament rails: surface energy and morphology transition. *J Colloid Interface Sci*. 341(2):326–332.
24 Bedarkar A, Wu XF, Vaynberg A. 2010. Wetting of liquid droplets on two parallel filaments. *Appl Surf Sci*. 256(23):7260.
25 Duprat C, Protière S, Beebe AY, Stone HA. 2012. Wetting of flexible fibre arrays. *Nature*. 482(7386):510.
26 Protiere S, Duprat C, Stone HA. 2013. Wetting on two parallel fibers: drop to column transitions. *Soft Matter*. 9(1):271.
27 Sauret A, Boulogne F, Cébron D, Dressaire E, Stone HA. 2015. Wetting morphologies on an array of fibers of different radii. *Soft Matter*. 11(20):4034–4040.
28 Boulogne F, Sauret A, Soh B, Dressaire E, Stone HA. 2015. Mechanical tuning of the evaporation rate of liquid on crossed fibers. *Langmuir*. 31(10):3094–3100.
29 Duprat C, Protiere S. 2015. Capillary stretching of fibers. *Europhys Lett*. 111(5):56006.
30 Pan Z, Weyer F, Pitt WG, Vandewalle N, Truscott TT. 2018. Drop on a bent fibre. *Soft Matter*. 14(19):3724–3729.
31 Aziz H, Tafreshi HV. 2019. Competing forces on a liquid bridge between parallel and orthogonal dissimilar fibers. *Soft Matter*. 15(35):6967–6977.
32 Wang F, Schiller UD. 2021. Hysteresis in spreading and retraction of liquid droplets on parallel fiber rails. *Soft Matter*. 17(22):5486–5498.
33 Bico J, Roman B, Moulin L, Boudaoud A. 2004. Adhesion: elastocapillary coalescence in wet hair. *Nature*. 432(7018):690.
34 Weyer F, Lismont M, Dreesen L, Vandewalle N. 2015. Compound droplet manipulations on fiber arrays. *Soft Matter*. 11(36):7086–7091.
35 Weyer F, Duchesne A, Vandewalle N. 2017. Switching behavior of droplets crossing nodes on a fiber network. *Sci Rep*. 7(1):1–9.
36 Charpentier JB, Brändle de Motta JC, Ménard T. 2020. Capillary phenomena in assemblies of parallel cylindrical fibers: from statics to dynamics. *Int J Multiph Flow*. 129:103304.
37 Luo C, Heng X, Xiang M. 2014. Behavior of a liquid drop between two nonparallel plates. *Langmuir*. 30(28):8373–8380.
38 Koulago A, Shkadov V, Quéré D, de Ryck A. 1995. Film entrained by a fiber quickly drawn out of a liquid bath. *Phys Fluids*. 7(6):1221–1224.